J. Chem. Sci. (2018) 130:14
https://doi.org/10.1007/s12039-017-1413-0

REGULAR ARTICLE

$NiFe_2O_4$ nanoparticles-decorated activated carbon nanocomposite based electrochemical sensor for selective detection of dopamine in presence of uric acid and ascorbic acid

T K APARNA and R SIVASUBRAMANIAN*

Electrochemical Sensor and Energy Materials Laboratory, Department of Chemistry, PSG College of Technology, Coimbatore, Tamilnadu 641 004, India
E-mail: rss@psgias.ac.in

MS received 22 August 2017; revised 9 December 2017; accepted 9 December 2017; published online 7 February 2018

Abstract. We propose an electrochemical sensor using $NiFe_2O_4$ nanoparticles-decorated activated carbon (AC) nanocomposite for selective detection of dopamine (DA) in the presence of uric acid (UA) and ascorbic acid (AA). The nanocomposite was prepared by a simple hydrothermal method and the characterization was done using transmission electron microscope (TEM), scanning electron microscope (SEM), X-ray diffraction (XRD) patterns and Fourier transform infrared (FTIR) spectroscopy. The $NiFe_2O_4$-AC-modified glassy carbon electrode (GCE) showed excellent electrocatalytic activity towards DA compared to $NiFe_2O_4$/GCE and AC/GCE. This is attributed to the synergistic action and the large surface area of the nanocomposite. Differential pulse voltammetry (DPV) was employed for the detection of DA wherein the detection limit of 0.4 μM along with a linear range of 5 μM to 100 μM was deduced. The selective detection of DA in presence of AA and UA was demonstrated. The advantages of the present sensor include the ease of preparation of the nanocomposite, low detection limit, remarkable selectivity, good reproducibility and stability.

Keywords. Electrochemical sensor; dopamine; cyclic voltammetry; differential pulse voltammetry; activated carbon.

1. Introduction

4-(2-Aminoethyl) benzene-1,2-diol, commonly known as dopamine (DA), belongs to the catecholamine family and is an important neurotransmitter responsible for controlling muscular activity and electrical impulses of the nerve cells.[1] DA is produced in the midbrain region, namely '*Substantia nigra*' of the human body. DA is synthesized by decarboxylation of 3,4-dihydroxy phenylalanine and serves as a precursor for the preparation of epinephrine (EP) and norepinephrine (NP). Generally, DA is present at very low concentration levels *viz.*, 10^{-6} M to 10^{-8} M in the human body. Abnormal levels of DA may lead to neurological disorders such as Parkinson's disease, schizophrenia, epilepsy, *etc*. In addition, DA is also employed to treat myocardial infarction and hypertension.[2] Hence it is essential to develop an analytical method to estimate DA in a facile and simple manner. Various techniques were developed to determine DA such as chromatography,[3] electrophoresis,[4] fluorescence spectroscopy[5] and electrochemical methods.[6] Apart from the electrochemical method, all other techniques mentioned above, suffer from cumbersome experimental procedures. On the other hand, electrochemical method is easy to operate, has a fast response time and does not require any stringent experimental conditions.

It is well-known that uric acid (UA) and ascorbic acid (AA) co-exist along with DA in cellular fluids. Both UA and AA serve as potential interfering species in the electrochemical detection of DA as they undergo oxidation at a potential near to that of DA. Hence, it is necessary to develop a selective and sensitive method for the determination of DA. In this context, nanomaterials due to its versatile properties were widely studied in recent years. Tremendous efforts were carried out using various nanomaterials such as polymers,[7–9] metal nanoparticles,[10–15] core@shell nanostructures,[16,17] alloys,[18,19] two-dimensional layered materials,[20–22] carbon based[23–26] and metal/metal oxide

---

*For correspondence

Electronic supplementary material: The online version of this article (https://doi.org/10.1007/s12039-017-1413-0) contains supplementary material, which is available to authorized users.

nanocomposites.[27–36] Yin *et al.*, reported a three-dimensional MoS_2 nanosheet for simultaneous detection of DA, UA and AA.[37] The peak separation for AA-DA, DA-UA and AA-UA were found to be 208.3 mV, 128.0 mV and 336.3 mV, respectively. Similarly, two-dimensional hexagonal boron nitride nanosheets supported on various carbon electrodes such as glassy carbon, screen-printed electrode (SPE) *etc*., was reported by Banks *et al.*[38] Though the electrode could easily differentiate DA and UA, it could not possibly resolve DA and AA. In a similar work, copper(I) oxide nanohexagon-reduced graphene oxide nanocomposite[39] was reported for selective detection of DA. A detection limit of 50 nM and a linear range from 10 to 900 μM was achieved.

Activated carbon (AC) with the high specific surface area and tunable porosity are mainly used in energy, sensor and environmental applications.[40] AC is a porous material with hydrophobic graphene layers and hydrophilic functional groups (OH^-/-COOH) present on the surface. They are generally derived from hydrocarbons. Many methods are available in the literature for activation of carbon.[41] Among them, chemical activation was found to be efficient and mostly preferred. Chemical activation was generally performed in alkaline medium and such activated carbon shows enhanced catalytic activity and better performance. Recently, Chitravathi and Munichandriah [42] prepared AC based carbon paste electrode for simultaneous determination of catecholamines. The activation was done by electrochemical method and the sensor showed better response towards detection. Similarly, Veeramani *et al.,*[43] reported a biomass-derived porous AC for detection of neurotransmitters. It was inferred that the use of AC improves the performance of the sensor.

In recent years, transition elements based mixed metal oxides have received considerable attention for diverse applications such as energy,[44] thermoelectricity,[45] *etc*. The presence of two metals in the structure with varying ratios help in tuning the properties of the material. In nickel ferrite, the Ni ion occupies the octahedral site and a half of the tetrahedral site; the remaining tetrahedral site is occupied by Fe. To the best of our knowledge, only a few reports pertaining to the sensing application of $NiFe_2O_4$ are available in the literature. For instance, Afkhami *et al.,*[46] showed $NiFe_2O_4$-graphene nanocomposite for effective determination of tramadol and acetaminophen, which are pharmaceutically important drug molecules. In another study, Ensafi *et al.,* reported the $NiFe_2O_4$ decorated multiwalled carbon nanotube (MWCNT) based sensor for efficient detection of DA.[47] From these studies, it was observed that the nanoparticle when supported on a carbon matrix, renders high stability with good catalytic activity. It is of interest to probe the performance of $NiFe_2O_4$ nanoparticles-decorated AC based nanocomposite for the detection of dopamine in the presence of interfering species. Herein, we report a $NiFe_2O_4$-AC based nanocomposite for selective determination of DA. The performance of the sensor towards dopamine was expected to enhance due to the synergistic action and the large surface area of the nanocomposite. The nanocomposite was prepared by a simple hydrothermal method and their electrocatalytic activity towards DA oxidation was demonstrated. Also, selective determination of DA in the presence of AA and UA was carried out. The sensor showed good reproducibility, stability and was successfully employed to detect DA in biological samples.

2. Experimental

2.1 *Chemicals*

$NiCl_2$ (≥ 99%, Merck), $FeCl_3$ (≥99%, Merck), Activated Carbon (Merck), NaOH (≥ 99%, Merck), Ethanol (Merck), Dopamine hydrochloride (≥ 98%, Himedia), AA (≥ 99%, Lobachem), UA (≥ 99%, Himedia), K_2HPO_4 (≥ 98%, Merck), KH_2PO_4 (≥ 98%, Merck), KNO_3 (≥ 98%, Merck), KCl (≥ 98%, Merck) and Urea (≥ 98%Merck) were used as received. Millipore water with a resistivity of 18 MΩ cm was employed for the preparation of the solutions.

2.2 *Synthesis of $NiFe_2O_4$-AC nanocomposite*

Briefly, 0.023 g of $NiCl_2$ and 0.054 g of $FeCl_3$ was dissolved in 30 mL of distilled water, followed by the addition of 0.04 g of NaOH. To the solution, 0.05 g of AC was added and the mixture was stirred for 10 min. The solution was then transferred to a tightly sealed Teflon-lined autoclave and placed in an oven at 180 °C for 15 h. The resulting solution was centrifuged, washed with ethanol and dried at 100 °C. A control experiment without the presence of AC was also carried out.

2.3 *Material Characterization*

The morphology of the synthesized nanocomposite was characterized using transmission electron microscope (TEM) (JEOL JEM 2100, Japan) and scanning electron microscope (SEM) (Carl Zeiss EVO-18, Germany). The presence of chemical constituents was confirmed through energy dispersive X-ray (EDX) analysis. The crystal structure was elucidated using X-ray diffraction (XRD) patterns from Bruker D8 Advance equipped with Cu Kα radiation source. Further, the characteristic formation of the nanocomposite was confirmed through Fourier transform infrared (FTIR) spectroscopy using Shimadzu FTIR spectrophotometer IR affinity 1S.

2.4 *Electrochemical Measurements*

The electrochemical investigations were performed from a three-electrode cell assembly. Electrochemical measurements such as cyclic voltammetry (CV), electrochemical impedance spectroscopy (EIS) and differential pulse voltammetry (DPV) were carried out using Model CHI 600E (CH Instruments USA). The glassy carbon electrode (GCE) with geometric area 0.07 cm^2 was employed as the working electrode and the Pt wire and Ag/AgCl (3 M KCl) was employed as a counter and reference electrode respectively. The electrochemical studies were performed by modifying the GCE using $NiFe_2O_4$-AC nanocomposite. Prior to modification, the GCE was cleaned with various grades of alumina (0.3 micron and 1 micron). 1 mg of $NiFe_2O_4$-AC nanocomposite was dispersed in 5 mL ethanol and 10 μL of the sample was dropcasted on the clean glassy carbon surface. The $NiFe_2O_4$-AC/GCE constitutes the working electrode. The modified electrode was characterized using EIS analysis. The Nyquist plot was recorded in the open circuit voltage (OCV) which is ∼0.3 V at an amplitude of 10 mV from a solution of 0.1 M PBS and 10 mM of $K_4[Fe(CN)_6]$. The frequency was varied between 1 x 10^5 Hz to 1 Hz. The electrocatalytic response for dopamine was studied using CV from a solution of 0.1 mM DA and 0.1 M PBS (phosphate buffer saline) solution. The potential was scanned between -0.2 V to 0.8 V (vs Ag/AgCl) with the scan rate fixed at 100 $mV\,s^{-1}$. The experiments were also repeated for $NiFe_2O_4$/GCE and AC/GCE under identical condition. The electrochemical sensing of dopamine was carried out using DPV on $NiFe_2O_4$-AC/GCE from 0.1 M PBS. The DPV measurements were recorded with the pulse width, pulse amplitude and pulse period being 0.05 s, 0.05 V and 0.5 s, respectively. A 10 mM stock solution of DA was prepared and various aliquots were added to the electrochemical cell. The DPV curves were recorded in the potential range -0.2 V to 0.5 V. Also, the selective detection of DA in presence of UA and AA were carried out from DPV under similar conditions.

2.5 *Analysis of real samples*

The determination of DA, UA and AA in serum and urine sample was analyzed using $NiFe_2O_4$-AC/GCE. The samples were obtained from male volunteers in the age groups of 25–30. 100 μL of the sample was diluted 50 times in 0.1 M PBS and various concentrations of analyte were spiked in the mixture. The calibration plot obtained earlier was used to estimate the amount of analyte in the samples. The experiments were repeated three times for each measurement.

3. Results and Discussion

3.1 *Characterization studies*

Figure 1 shows the XRD patterns of $NiFe_2O_4$, AC and $NiFe_2O_4$-AC nanocomposite. For $NiFe_2O_4$ the peaks at 14.4°, 33.4°, 35.7°, 43.8°, 53.8°, 57.2°, and 63.1° could be indexed to (111), (220), (311), (400), (422), (511) and (440) planes, respectively. This confirms the presence of cubic inverse spinel structure of $NiFe_2O_4$ having Fd3m space group. The values were consistent with JCPDS reference no. 54-0964. Also, the absence of any secondary peaks indicates the formation of single phase structure with high purity. In the case of AC, the broad peak at 25° reflects the (002) plane of graphitic framework indicating the amorphous nature of AC. On the other hand, for the nanocomposite, the diffraction peaks corresponding to both AC and $NiFe_2O_4$ were observed which indicates the rigid adherence of $NiFe_2O_4$ on the AC surface. Further, the formation of $NiFe_2O_4$-AC was studied using FTIR spectroscopy as shown in Figure S1 (in the Supplementary Information). The bands at 3430.0 cm^{-1} and 1645.7 cm^{-1} for $NiFe_2O_4$ correspond to the stretching vibration of free and adsorbed water molecule. The peak at 593.2 cm^{-1} corresponds to the stretching vibration of metal at the tetrahedral sites (Fe-O). In the case of AC, the band at 1561.1 cm^{-1} can be indexed to C=C stretching vibration of graphitic carbon and a small peak around 3200 cm^{-1} can be due to the stretching vibration of the hydroxyl group present on the surface of the AC. For the nanocomposite, a red shift was observed for the Fe-O stretching vibration from 593.2 cm^{-1} to 597.8 cm^{-1} and similarly, the

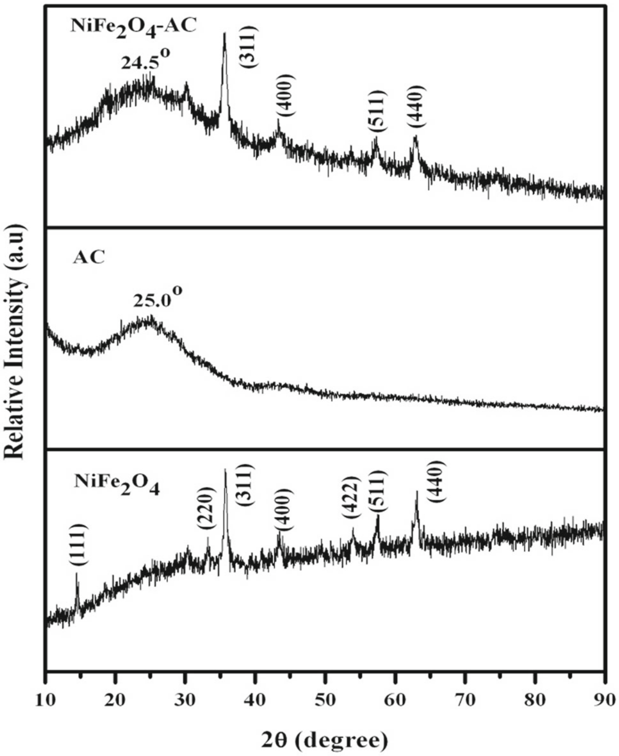

Figure 1. XRD patterns of $NiFe_2O_4$, AC and $NiFe_2O_4$-AC nanocomposite.

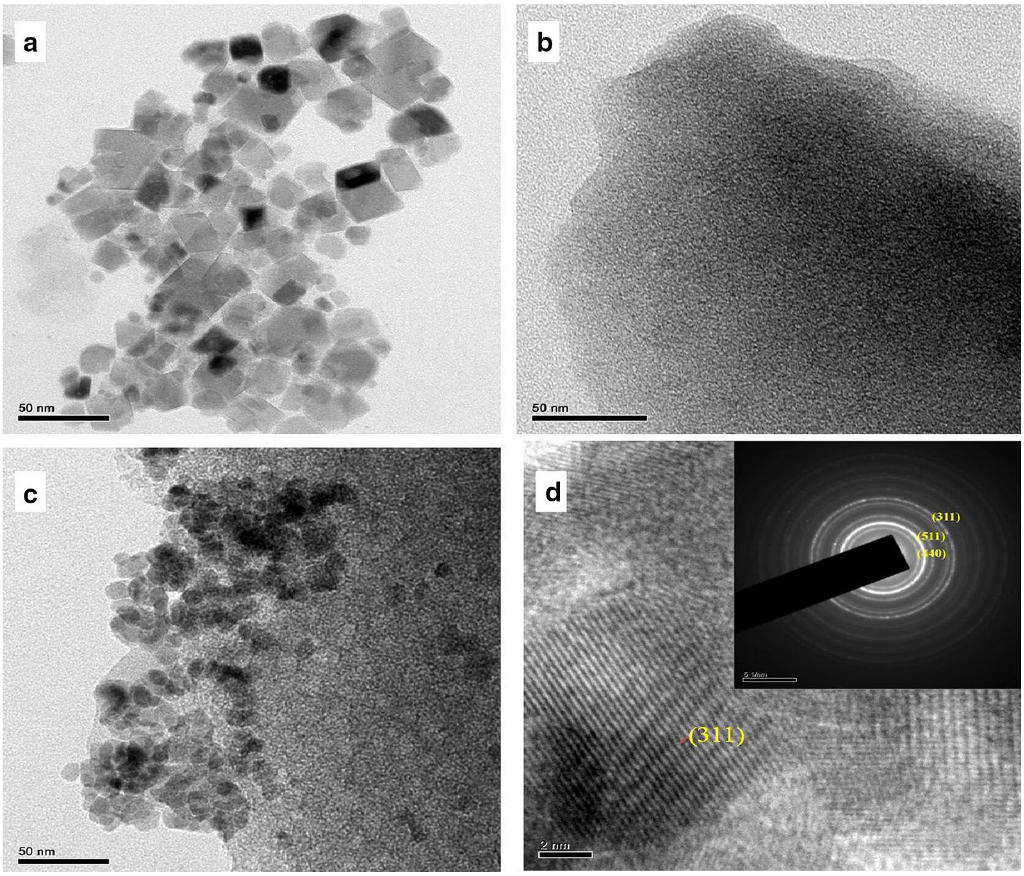

Figure 2. TEM images of (a) $NiFe_2O_4$, (b) AC, (c) $NiFe_2O_4$-AC prepared from a simple hydrothermal method, and (d) HRTEM image of $NiFe_2O_4$-AC depicting the lattice fringes of (311) plane of $NiFe_2O_4$. The inset depicts the SAED pattern of the nanocomposite.

C=C vibration showed a blue shift from 1561.1 cm^{-1} to 1549.8 cm^{-1}. This shift can be attributed to the electrostatic attraction between the $NiFe_2O_4$ nanoparticles and the functional groups present on the surface of AC in the nanocomposite.

Figure 2 depicts the TEM image of $NiFe_2O_4$, AC and $NiFe_2O_4$-AC nanocomposite. The typical TEM image of $NiFe_2O_4$ (Figure 2a) depicts polygonal morphology with diverse shapes. The dimension of the particles lies between 10 to 30 nm. With the addition of NaOH, the metal precursor forms their corresponding hydroxides and the subsequent heat treatment results in co-precipitation of $NiFe_2O_4$ nanoparticles. Figure 2b shows the TEM image of AC, sheet-like structures with a few stacked layers were observed. Figure 2c depicts the TEM image of $NiFe_2O_4$-AC nanocomposite wherein the $NiFe_2O_4$ nanoparticles were found to be strongly anchored on the carbon surface. It is found that there is a change in morphology of $NiFe_2O_4$ nanoparticles (Figure 2c) which could be attributed to the incorporation of the support matrix (AC), thereby leading to more proximity of the nanoparticles resulting in aggregation. The HRTEM image in Figure 2d explicitly shows the lattice fringe patterns and the inset depicts the SAED image with a bright spot and ring pattern. The spot pattern specifies the crystalline nature of $NiFe_2O_4$ and the ring pattern reflects the amorphous nature of AC. The interplanar distances measured from the HRTEM image were well in correlation with the SAED pattern. The SEM image of the nanocomposite was shown in Figure S2 (Supplementary Information). The elemental mapping for C, Ni, Fe and O were performed and the EDX analysis reveals the distribution of all the elements in the nanocomposite with their approximate stoichiometry (Ni – 9.69%, Fe – 18.09%, O – 36.04% and C - 35.26%).

The interfacial behavior of the modified electrode can be well understood using EIS analysis. In EIS, a constant potential (generally OCV) was applied and the impedance was measured from high frequency to low frequency region. Typically, the impedance was represented by Nyquist plot wherein the variation of real part of impedance to the imaginary part was recorded. The Nyquist plot exhibits a semicircle in the high-frequency region followed by a vertical spike. The diameter of the semicircle gives the charge transfer

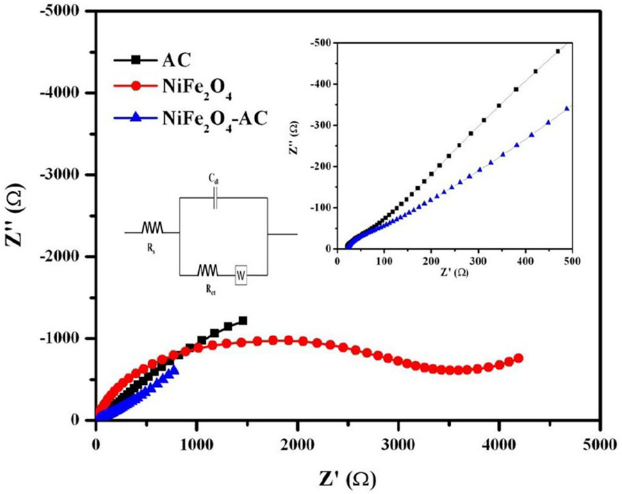

Figure 3. Nyquist plot of $NiFe_2O_4$, AC and $NiFe_2O_4$-AC nanocomposite from a solution containing 10 mM of $K_4Fe(CN)_6$ and 0.1 M PBS solution in the frequency range of 1 x 10^5 Hz to 1 Hz. The inset depicts the enlarged image of AC and $NiFe_2O_4$-AC and the corresponding equivalent circuit fitted for the Nyquist plots.

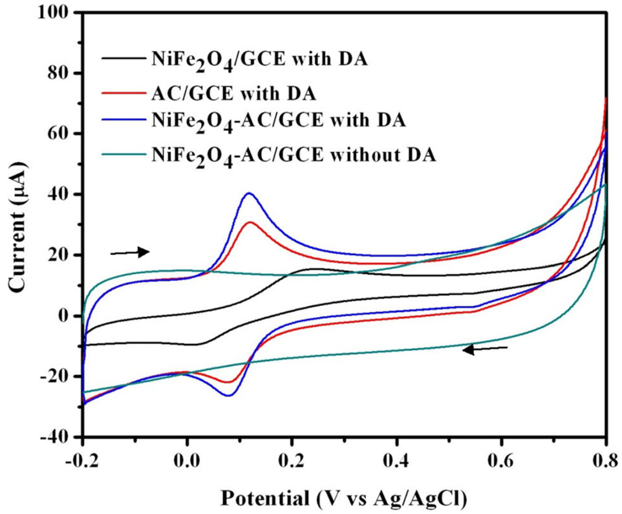

Figure 4. Cyclic voltammogram of $NiFe_2O_4$/GCE, AC/GCE and $NiFe_2O_4$-AC/GCE from a solution containing 0.1 M PBS and 0.1 mM DA at a scan rate of 100 mV s^{-1}. The arrow marks in the CV curves indicate the sweep directions.

resistance (R_{ct}) and the vertical spike corresponds to the Warburg impedance. Herein, the Nyquist plots were recorded for $NiFe_2O_4$/GCE, AC/GCE and $NiFe_2O_4$-AC/GCE from 0.1 M PBS and 10 mM $K_4[Fe(CN)_6]$ at their OCV (∼0.3 V) (Figure 3). The equivalent circuit was obtained from which the impedance parameters have been extracted and is provided in Table S1 (Supplementary Information). It is found that the R_{ct} values were 3517.00 Ω, 43.05 Ω and 14.46 Ω for $NiFe_2O_4$/GCE, AC/GCE and $NiFe_2O_4$-AC/GCE, respectively. The R_{ct} is lower for the nanocomposite, which indicates its good conductivity and electron transfer ability compared to other modified systems.

In addition, the electrochemical active surface area of the modified electrode was calculated from the CV response in a solution of 0.1 M PBS and 1 mM $K_4[Fe(CN)_6]$ at a scan rate of 0.1 mV s^{-1}. The active surface area was calculated using the Randles-Sevcik equation and is found to be 0.120 cm^2, 0.362 cm^2 and 0.530 cm^2 for $NiFe_2O_4$/GCE, AC/GCE and $NiFe_2O_4$-AC/GCE. The CV response of the modified electrode and the estimated surface area is provided in Figure S3 and Table S2 (Supplementary Information). From the estimated values, it was found that, with the addition of $NiFe_2O_4$ to AC, the total surface area of the nanocomposite increases.

3.2 *Electrooxidation of DA*

The electrooxidation behavior of DA was investigated using CV from 0.1 M PBS (pH = 7.0) and 0.1 mM DA at a scan rate of 100 mV s^{-1}. Figure 4 shows the CV response for $NiFe_2O_4$/GCE, AC/GCE and $NiFe_2O_4$-AC/GCE with and without the addition of DA. The redox peaks at around ∼0.12 V and ∼0.08 V was observed for all the electrodes. From the Figure 4, it is clear that the $NiFe_2O_4$-AC/GCE showed enhanced oxidation activity compared to AC/GCE and $NiFe_2O_4$/GCE. The difference between the cathodic and anodic peak potentials (ΔE_p) for $NiFe_2O_4$-AC/GCE was 30 mV which was smaller compared to AC/GCE (42 mV) and $NiFe_2O_4$/GCE (240 mV) indicating a fast reaction kinetics for dopamine on the nanocomposite modified electrode. Also, the cathodic and anodic peak currents were higher for the nanocomposite compared to other electrodes. The high activity arises due to the synergistic action along with the increased surface area of the nanocomposite. In addition, the $NiFe_2O_4$ nanoparticles prevent the fouling of electrode surface during the reaction.

In order to study the electrochemical kinetics for dopamine oxidation, CV curves were recorded at various scan rates ranging from 100 mV s^{-1} to 1000 mV s^{-1} (Figure 5a). The peak current increases with the increase in scan rate and the corresponding calibration plot are shown in Figure 5b. The linear fit indicates that, the oxidation of dopamine on $NiFe_2O_4$-AC/GCE is an adsorption controlled process. The corresponding linear regression equation is as follows:

$$I_{pa}(\mu A) = 151.7\ \nu(V\ s^{-1}) + 34.0(R^2 = 0.9641) \quad (1)$$

$$I_{pc}(\mu A) = -163.1\ \nu(V\ s^{-1}) - 18.0(R^2 = 0.9736) \quad (2)$$

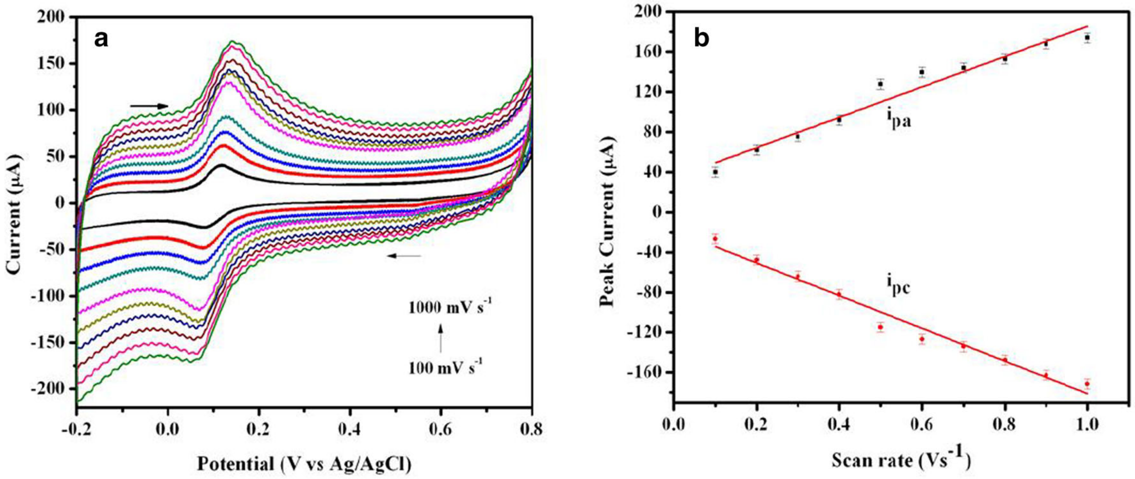

Figure 5. (a) The cyclic voltammetric responses of $NiFe_2O_4$-AC/GCE in 0.1 M PBS and 0.1 mM dopamine at different scan rates ranging from 100 mV s^{-1} to 1000 mV s^{-1}, and (b) their corresponding calibration plots.

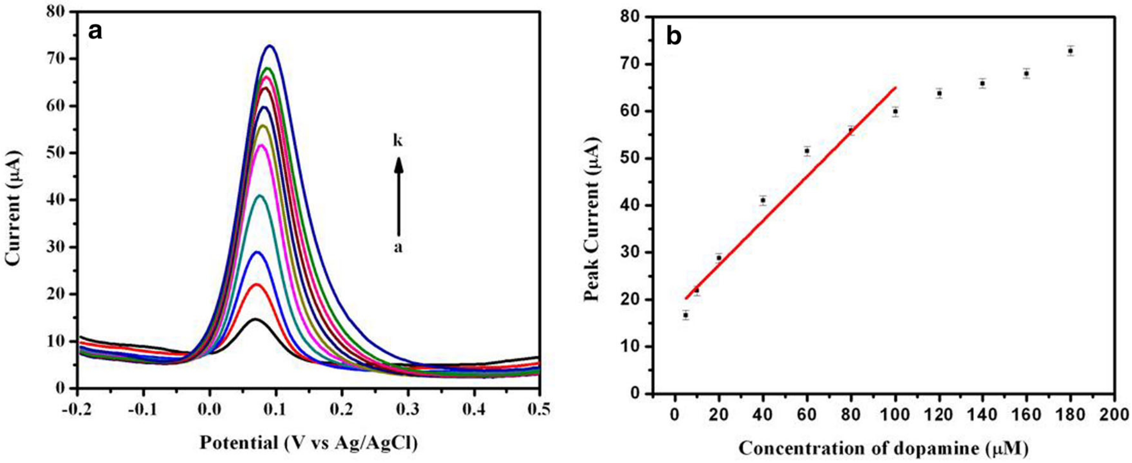

Figure 6. (a) Differential pulse voltammetric responses of $NiFe_2O_4$-AC/GCE from 0.1 M PBS at different concentrations of dopamine: (a) 5 μM, (b) 10 μM, (c) 20 μM, (d) 40 μM, (e) 60 μM, (f) 80 μM, (g) 100 μM, (h) 120 μM, (i) 140 μM, (j) 160 μM and (k) 180 μM; and (b) the calibration plot.

3.3 *Electrochemical detection of DA*

The sensing of DA was carried out using DPV from 0.1 M PBS at pH 7. DPV is an effective analytical technique for trace level detection of the analyte. A 10 mM stock solution of DA was prepared and various aliquot of DA was added for successive measurements. The potential was scanned between -0.2 V to 0.5 V. Figure 6a shows the DPV curve for DA oxidation for the concentration of 5 μM to 180 μM. The DPV curves were depicted after performing the necessary background correction from the blank voltammogram (without the addition of DA). The peak current increases with increase in concentration and the calibration plot (Figure 6b) was constructed from the DPV peak current. The plot shows linearity from 5 μM to 100 μM with the linear regression equation, given as,

$$I_p\,(\mu A) = 0.47\,C_{DA}\,(\mu M) + 17.9\ (R^2 = 0.9489) \quad (3)$$

The limit of detection (LOD) was estimated as 0.4 μM using the formula[48] LOD = 3s/m where s is the standard deviation of the blank voltammogram (0.063 μA) and m is the slope of the calibration curve (0.47 μA μM^{-1}). The estimation of the standard deviation of blank voltammogram (Figure S4 in SI) and the details pertaining to the calculation of the detection limit are provided in the Supplementary Information.

3.4 *Selective detection of DA in presence of UA and AA*

The selective detection of DA in presence of UA and AA was performed on $NiFe_2O_4$-AC/GCE in 0.1 M PBS

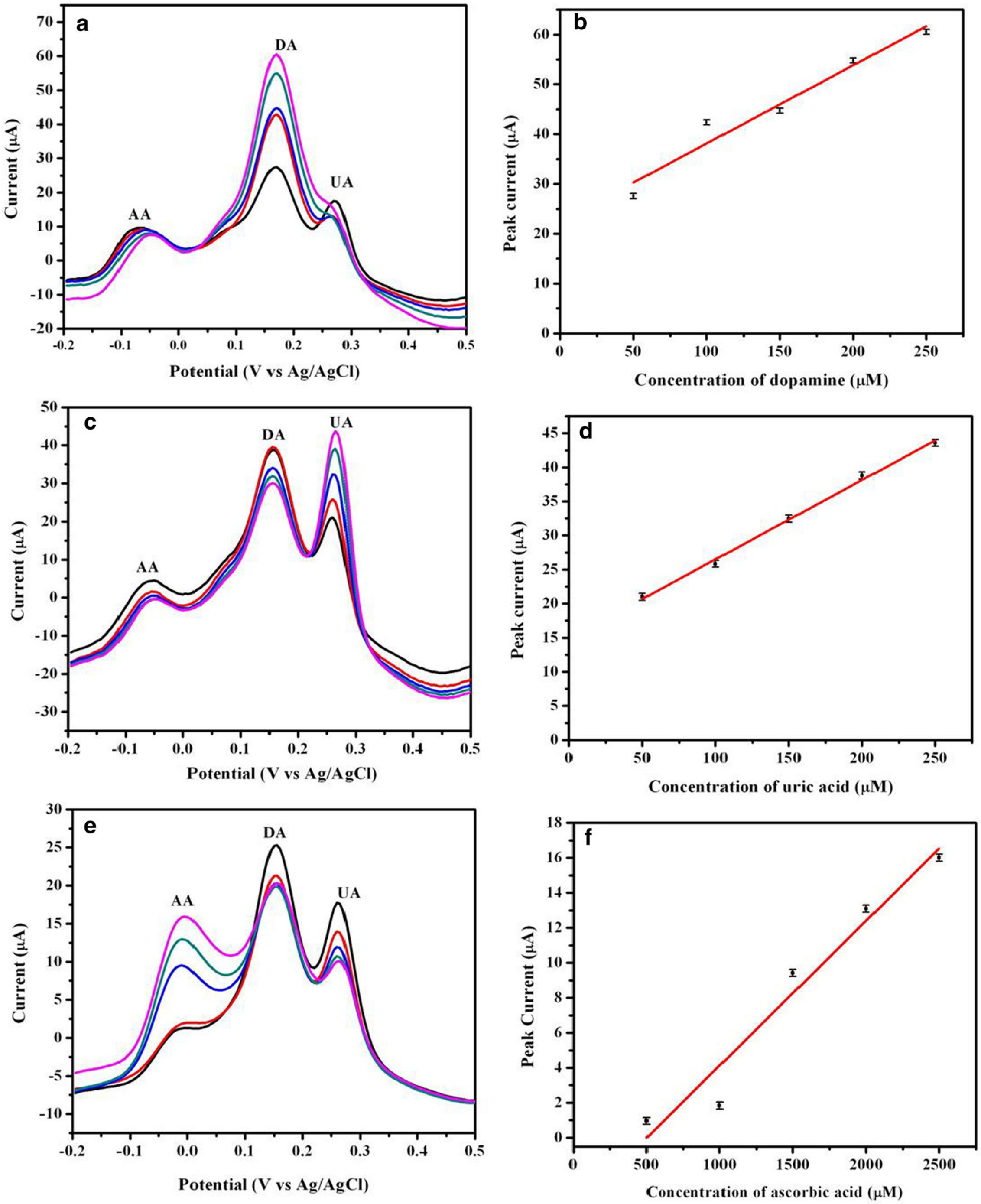

Figure 7. Differential pulse voltammetric responses on $NiFe_2O_4$-AC/GCE in 0.1 M PBS at different concentrations of, (a) DA (50 μM to 250 μM), (c) UA (50 μM to 250 μM) and (e) AA (500 μM to 2500 μM); (b,d,f) the corresponding calibration plots.

as shown in Figure 7. As it is a ternary mixture, the concentration of one molecule was varied with the other two kept constant. Figure 7a shows the DPV curves for the variation of DA from 50 μM to 250 μM while the concentration of UA and AA was fixed at 50 μM and 2500 μM, respectively. Three well-defined peaks for AA, DA and UA were obtained and the peak separation for AA-DA, DA-UA and AA-UA were obtained as 247.0 mV, 101.0 mV and 348.0 mV, respectively. This large peak separation was good enough to detect all the three molecules simultaneously. A calibration plot was constructed as shown in Figure 7b with the linear regression equation as,

$$I_p\ (\mu A) = 0.156\ C_{DA}\ (\mu M) + 22.45\ (R^2 = 0.9699) \tag{4}$$

Similarly, the experiments were repeated by changing the concentration of UA from 50 μM to 250 μM (Figure 7c) while keeping the concentration of DA and AA at 100 μM and 2500 μM. The peak current corresponding to UA increases with concentration (Figure 7d) and the linear regression equation is given as,

$$I_p\ (\mu A) = 0.116\, C_{UA}\ (\mu M) + 14.8\ (R^2 = 0.9955) \quad (5)$$

It is known that the detection of DA is affected in the presence of high concentration of AA.[49] Hence, it is a challenging task to detect DA in presence of high concentration of AA. Figure 7e shows the DPV curves recorded with increasing the concentration of AA from 500 μM to 2500 μM. The concentration of DA and UA was maintained as 100 μM and 50 μM. Interestingly, the presence of high concentration of AA does not affect the DPV peaks of DA and UA significantly. Figure 7f shows the calibration plot and the linear regression equation is given as,

$$I_p\ (\mu A) = 0.008\ C_{AA}\ (\mu M) - 4.14\ (R^2 = 0.9394) \quad (6)$$

Table 1 provides a comparative account on the performance of various sensors employed for detection of DA, UA and AA. The present electrochemical sensor exhibited satisfactory performance in terms of linear range and peak separation. The presence of hydroxyl and carboxyl functional groups imparts a negative charge on the carbon surface which attracts the positively charged DA (pKa = 8.9) and repels negatively charged UA (pKa = 3.9) and AA (pKa = 4.1). Also, the DPV signal was not affected in the presence of a five-fold excess concentration of K^+, Na^+, Cl^-, SO_4^- ions and urea solution. However, with the addition of glucose, the peak current of DA increases as glucose gets oxidized at the same potential as that of DA. Further work is in progress to improve the selectivity of the sensor in the presence of glucose.

3.5 *Reproducibility and stability*

The reproducibility of the $NiFe_2O_4$-AC/GCE was investigated for ten successive measurements of DA. The sensor showed a good response with the standard deviation of 3.7%. The stability of the sensor was analyzed using CV. The CV response for 0.1 mM DA in 0.1 M PBS was recorded for 100 cycles and it was found that the oxidation peak current for DA retained 90% of the initial value after 100 cycles. The long-term stability of the sensor was examined using DPV from a solution of 0.1 mM DA and 0.1 M PBS. The DPV current was measured for 0, 7, 14 and 21 days using the same modified electrode. The electrode was stored in PBS solution

Table 1. A comparison on the performance of various dopamine biosensors.

S. No	Material	Method	Limit of detection (μM)			Linear range (μM)			Peak separation (mV)			References
			DA	UA	AA	DA	UA	AA	DA-AA	DA-UA	AA-UA	
1	rGO/ZnO	DPV	1.08	0.33	3.71	3–330	1–70	50–2350	236	132	368	50
2	MoS_2	DPV	0.15	0.82	0.06	5–1200	1–900	1–60	208	128	336	37
3	SnO_2/rGO	DPV	0.006	–	–	0.08–30	–	–	200	120	320	27
4	NSG-Fe_2O_3	DPV	0.03	–	–	0.3–210	–	–	250	–	–	51
5	SnO_2/Ch	DPV	0.77	0.89	6.45	1–18	1–100	20–220	178	337	592	52
6	CB /Ch	DPV	0.1	0.1	0.1	0.1–1400	5-1800	25-1600	190	240	330	53
7	$NiFe_2O_4$/MWCNT	DPV	0.02	–	–	0.5–6	–	–	–	–	–	47
8	e-FGP	DPV	2	0.01	0.02	0.5–35	0.5–35	20–400	210	340	330	54
9	ERGO/GCE	DPV	0.5	0.5	–	0.5–60	0.5–60	500–2000	240	130		55
10	$NiFe_2O_4$-AC/	DPV	0.4	–	–	5–100	50–250	500–2500	247	101	348	This work

rGO reduced graphene oxide, *NSG* nitrogen,sulphur doped graphene, *Ch* Chitosan, *MWCNT* Multiwalled carbon nanotube, *e-FGP* Exfoliated flexible graphene paper, *ERGO* Electrochemically reduced graphene oxide.

Table 2. Estimation of DA, UA and AA in biological samples using $NiFe_2O_4$-AC/GCE in 0.1 M PBS.

Amount added (μM)			Amount estimated (μM)					
DA	UA	AA	DA	% of recovery	UA	% of recovery	AA	% of recovery
Serum								
50	50	500	50.8	101.6±2	49.2	98.4±3	501	100.2±3
100	100	1000	99.8	99.8±3	98.5	98.5±4	1012	101.2±2
150	150	1500	149.3	99.5±1	148.7	99.1±2	1510	100.6±5
Urine								
50	20	500	49.6	99.2±1	19.9	99.5±2	498	99.6±2
100	50	1000	98.7	98.7±2	50.4	100.8±2	995	99.5±4
150	150	1500	148.8	99.2±1	149.7	99.8±3	1495	99.6±2

during the long-term measurements. The oxidation current retained 85% of the initial value after 21 days. These findings illustrate the excellent reproducibility and long-term stability of the proposed sensor.

3.6 *Estimation of DA, UA and AA in real samples*

The validity of the sensor was studied by estimating DA, UA and AA on $NiFe_2O_4$-AC/GCE in human serum and urine samples. The biological sample was diluted 50 times in 0.1 M PBS and known amount of the analyte was spiked in the solution. The amount was estimated by comparing the DPV current with the calibration plot obtained earlier (Figure 6b). Table 2 indicates the amount of the analyte added and the amount estimated. The estimated values were in agreement with the spiked ones with good recovery values. The experiments have been repeated for three successive measurements and the values were satisfactory with a low standard deviation.

4. Conclusions

In this work, $NiFe_2O_4$ nanoparticles-decorated on AC-based nanocomposite were prepared by a simple hydrothermal method and the nanocomposite was characterized using SEM, TEM, XRD and FTIR spectroscopy. The microscopic studies revealed the distribution of $NiFe_2O_4$ nanoparticles on AC surface. The XRD indicates the formation of inverse spinel structure of $NiFe_2O_4$ and from the FTIR spectroscopy, the characteristic vibrations of the chemical bonds were inferred. The electrochemical activity of DA on $NiFe_2O_4$-AC/GCE was studied using CV. The nanocomposite exhibited increased activity compared to $NiFe_2O_4$/GCE and AC/GCE. The detection of DA was carried out using DPV wherefrom the LOD and linear range was estimated as 0.4 μM and 5 μM to 100 μM. Also, the selective detection of DA in the presence of AA and UA was accomplished. The validity of the sensor towards real sample analysis was examined. The advantage of this nanocomposite-modified electrode is the ease of its synthesis, low detection limit, long linear range and selective detection of dopamine in presence of UA and AA. This work can provide a better platform for the development of other mixed metal oxide based selective electrochemical sensors.

Supplementary Information

SEM images and FTIR spectrum of $NiFe_2O_4$-AC based nanocomposite, the impedance parameters obtained from Nyquist plots, the estimation of electrochemical active surface area and estimation of detection limit of the nanocomposite are available at www.ias.ac.in/chemsci.

Acknowledgements

This work was financially supported by the Department of Science and Technology (Grant No. ECR/2015/000099), Government of India. The authors wish to acknowledge the facilities and support provided by the Management PSG Sons and Charities, Coimbatore, India.

References

1. Dalley J W and Roiser J P 2012 Dopamine, serotonin and impulsivity *Neuroscience* **215** 42
2. Cao X, Luo L, Ding Y, Zou X and Bian R 2008 Electrochemical methods for simultaneous determination of dopamine and ascorbic acid using cetylpyridine bromide/chitosan composite film-modified glassy carbon electrode *Sens. Actuat. B-Chem.* **129** 941
3. Guan C L, Ouyang J, Li Q L, Liu B H and Baeyens W R G 2000 Simultaneous determination of catecholamines by ion chromatography with direct conductivity detection *Talanta* **50** 1197

4. Saylor R A, Reid E A and Lunte S M 2015 Microchip electrophoresis with electrochemical detection for the determination of analytes in the dopamine metabolic pathway *Electrophoresis* **36** 1912
5. Yildirim A and Bayindir M 2014 Turn-on fluorescent dopamine sensing based on in situ formation of visible light emitting polydopamine nanoparticles *Anal. Chem.* **86** 5508
6. Jackowska K and Krysinski P 2013 New trends in electrochemical sensing of dopamine *Anal. Bioanal. Chem.* **405** 3753
7. Yu Z, Li X, Wang X, Ma X, Li X and Cao K 2012 Voltammetric determination of dopamine and norepinphrine on a glassy carbon electrode modified with poly (L-aspartic acid) *J. Chem. Sci.* **124** 537
8. Kalimuthu P and John A S 2011 Selective determination of 3,4-dihydroxyphenylacetic acid in the presence of ascorbic and uric acids using polymer modified electrode *J. Chem. Sci.* **123** 349
9. Gualandi I, Tonelli D, Mariani F, Scavetta E, Marzocchi M and Fraboni B 2016 Selective detection of dopamine with an all PEDOT:PSS organic electrochemical transistor *Sci. Reports* **6** 35419
10. Kumar K M, Pratap R K V, Mohan S and Jha S K 2016 Preparation of electro-reduced graphene oxide supported walnut shape nickel nanostructures and their application to selective detection of dopamine *Microchim. Acta* **183** 1759
11. Kaur B, Pandiyan T, Satpati B and Srivastava R 2013 Simultaneous and sensitive determination of ascorbic acid, dopamine, uric acid and tryptophan with silver nanoparticles-decorated reduced graphene oxide modified electrode *Colloids Surf. B* **111** 97
12. Ramaraj R 2006 Nanostructured metal particle-modified electrode for electrocatalytic and sensor applications *J. Chem. Sci.* **118** 593
13. Raj C R, Tokuda K and Ohsaka T 2001 Electroanalytical applications of cationic self-assembled monolayers: square-wave voltammetric determination of dopamine and ascorbate *Bioelectrochem.* **53** 183
14. Raj C R, Okajima T and Ohsaka T 2003 Gold nanoparticle arrays for the voltemmetric sensing of dopamine *J. Electroanal. Chem.* **543** 127
15. Raj C R and Ohsaka T 2001 Electroanalysis of ascorbate and dopamine at a gold electrode modified with a positively charged self-assembled monolayer *J. Electroanal. Chem.* **496** 44
16. Choudhary M, Brink R, Nandi D, Siwal S and Mallick K 2017 Gold nanoparticle within polymer chain, a multifunctional complex material, for the electrochemical detection of dopamine, and the hydrogen atom-mediated reduction of Rhodamine B, a mechanistic approach *J. Mater. Sci.* **52** 770
17. Zhang W, Zheng J, Tan C, Lin X, Hu S, Chen J, You X and Li S 2015 Designed self-assembled hybrid Au@CdS core-shell nanoparticles with negative charge and their application as highly selective biosensors *J. Mater. Chem. B* **3** 217
18. Liu M, Chen Q, Lai C, Zhang Y, Deng J, Li H and Yao S 2013 A double signal amplification platform for ultrasensitive and simultaneous detection of ascorbic acid, dopamine, uric acid and acetaminophen based on a nanocomposite of ferrocene thiolate stabilized Fe_3O_4@Au nanoparticles with graphene sheet *Biosens. Bioelectron.* **48** 75
19. Zhao D, Fan D, Wang J and Xu C 2015 Hierarchical nanoporous platinum-copper alloy for simultaneous electrochemical determination of ascorbic acid, dopamine and uric acid *Microchim. Acta* **182** 1345
20. Hou J, Xu C, Zhao D and Zhou J 2016 Facile fabrication of hierarchical AuAg alloy and its highly sensitive detection towards dopamine and uric acid *Sens. Actuat. B-Chem.* **225** 241
21. Mani V, Govindasamy M, Chen S, Karthik R and Huang S 2016 Determination of dopamine using a glassy carbon electrode modified with graphene and carbon nanotube hybrid decorated with molybdenum disulfide flowers *Microchim. Acta* **183** 2267
22. Xing L and Ma Z 2016 A glassy carbon electrode modified with a nanocomposite consisting of MoS_2 and reduced graphene oxide for electrochemical simultaneous determination of ascorbic acid, dopamine and uric acid *Microchim. Acta* **183** 257
23. Nayak P, Kurra N, Xia C and Alshareef H N 2016 Highly efficient laser scribed graphene electrodes for on-chip electrochemical sensing applications *Adv. Mater.* **2** 1600185
24. Dong J, Hu Y, Zhu S, Xu J and Xu Y 2010 A highly selective and sensitive dopamine and uric acid biosensor fabricated with functionalized ordered mesoporous carbon and hydrophobic ionic liquid *Anal. Bioanal. Chem.* **396** 1755
25. Pruneanu S, Biris A R, Pogacean F, Socaci C, Coros M, Rosu M C, Watanabe F and Biris A R 2015 The influence of uric acid and ascorbic acid on the electrochemical detection of dopamine using graphene-modified electrodes *Electrochim. Acta* **154** 197
26. Aneesh K and Berchmans S 2017 Highly selective sensing of dopamine using carbon nanotube ink doped with anionic surfactant modified disposable paper electrode *J. Solid State Electrochem.* **21** 1263
27. Ma H, Chen T, Luo Y, Kong F, Fan D, Fang H and Wang W 2016 Electrochemical determination of dopamine using octahedral SnO_2 nanocrystals bound to reduced graphene oxide nanosheets *Microchim. Acta* **182** 2001
28. Roychoudhury A, Basu S and Jha S K 2016 Dopamine biosensor based on surface functionalized nanostrucutred nickel oxide platform *Biosens. Bioelectron.* **84** 72
29. Yasmin S, Ahmed M S, Park D and Jeon S 2016 Nitrogen-doped graphene supported cobalt oxide for sensitive determination of dopamine in presence of high level of ascorbic acid *J. Electrochem. Soc.* **163** B491
30. Baraneedharan P, Alexander S and Ramprabhu S 2016 One-step in situ hydrothermal preparation of grpahene-SnO_2 nanohybrid for superior dopamine detection *J. Appl. Electrochem.* **46** 1187
31. Zhang X, Zhang Y and Ma L 2016 One-pot facile fabrication of zinc oxide composite and its enhanced sensitivity for simultaneous electrochemical detection of ascorbic acid, dopamine and uric acid *Sens. Actuat. B-Chem.* **227** 448

32. Wu L, Tan Y, Wang L, Sun S, Qu Z, Zhang J and Fan Y 2015 Dopamine sensor based on hybrid material composed of cuprous oxide hollow microspheres and carbon black *Microchim. Acta* **182** 1361
33. Selvaraju T and Ramaraj R 2014 Signal amplification of dopamine using lanthanum hexacyanoferrate-modified electrode *J. Chem. Sci.* **126** 11
34. Xie Y, Yuan J, Ye H, Song P and Hu S 2015 Facile ultrasonic synthesis of graphene/SnO_2 nanocomposite and its application to the simultaneous electrochemical determination of dopamine, ascorbic acid and uric acid *J. Electroanal. Chem.* **749** 26
35. Sun W, Wang X, Wang Y, Ju X, Xu L, Li G and Sun Z 2013 Application of graphene- SnO_2 nanocomposite modified electrode for the sensitive electrochemical detection of dopamine *Electrochim. Acta* **87** 317
36. Anithaa A C, Lavanya N, Asokan K and Sekar C 2015 WO_3 nanoparticles based direct electrochemical dopamine sensor in the presence of ascorbic acid *Electrochim. Acta* **167** 294
37. Yin A, Wei X, Cao Y and Li H 2016 High-quality molybdenum disulphide nanosheets with 3D structure for electrochemical sensing *Appl. Surf. Sci.* **385** 63
38. Khan A F, Brownson D A C, Randviir E P, Simth G C and Bankd C E 2016 2D hexagonal boron nitride (2D-hBN) explored for the electrochemical sensing of dopamine *Anal. Chem.* **88** 9729
39. Sivasubramanian R and Biji P 2016 Preparation of copper (I) oxide nanohexagon decorated reduced graphene oxide nanocomposite and its application in electrochemical sensing of dopamine *Mater. Sci. Engg. B* **210** 10
40. Marsh H and Rodriguez-Reinso 2006 *Activated Carbon* (UK: Elseiver)
41. Kim B, Lee Y and Park S 2007 A study on pore-opening behavior of graphite nanofibers by a chemical activation process *J. Colloid Interface Sci.* **306** 454
42. Chitravathi S and Munichandraiah N 2015 Simultaneous determination of catecholamines in presence of uric acid and ascorbic acid at a highly sensitive electrochemically activated carbon paste electrode *J. Electrochem. Soc.* **162** B163
43. Veeramani V, Madhu R, Chen S, Lou B, Palanisamy J and Vasantha V S 2015 Biomass-derived functional porous carbons as novel electrode material for the practical detection of biomolecules in human serum and snail hemolymph *Sci. Sci. Reports* **5** 10141
44. Wang X, Yu L, Wu X, Yuvan F, Guo Y, Ma Y and Yao J 2009 Synthesis of single-crystalline Co_3O_4 octahedral cages with tunable size aperture and their lithium storage properties *J. Phys. Chem. C* **113** 1553
45. Rivas-Murias B, Vila-Fungueirino J M and Rivadulla F 2015 High quality thin films of thermoelectric misfit cobalt oxides prepared by a chemical reduction method *Sci. Reports* **5** 11889
46. Afkhami A, Khoshsafar H, Bagheri H and Madrakian T 2014 Preparation of $NiFe_2O_4$/graphene nanocomposite and its application as a modifier for the fabrication of an electrochemical sensor for simultaneous determination of tramadol and acetaminophen *Anal. Chim. Acta* **831** 50
47. Ensafi A A, Arashpour B, Rezaei B and Allafchian A R 2014 Voltammetric behavior of dopamine at a glassy carbon electrode modified with $NiFe_2O_4$ magnetic nanoparticles decorated with multiwalled carbon nanotubes *Mater. Sci. Engg. C* **39** 78
48. Skoog D A, Holler F J and Crouch S R 1998 In *Principles of Instrumental Analysis* 6th edn. (USA: Thomas Brooks/Cole) p. 20
49. How G T S, Pandikumar A, Ming H N and Ngee L H 2014 Highly exposed {001} facets of titanium dioxide modified with reduced graphene oxide for dopamine sensing *Sci. Reports* **4** 5044
50. Zhang X, Zhang Y and Ma L 2016 One-pot facile fabrication of graphene-zinc oxide composite and its enhanced sensitivity for simultaneous electrochemical detection of ascorbic acid, dopamine and uric acid *Sens. Actuat. B-Chem.* **227** 488
51. Yasmin S, Ahmed MS and Jeon S 2015 Determination of dopamine by dual doped graphene-Fe2O3 in presence of ascorbic acid *J. Electrochem. Soc.* **162** B363
52. Selvarajan S, Suganthi A and Rajarajan M 2017 A facile approach to the synthesis of mesoporous SnO_2/Chitosan nanocomposite modified electrode for simultaneous determination of ascorbic acid, dopamine and uric acid *Surf. Interfaces* **7** 146
53. Dinesh B, Saraswathi R and Senthilkumar A 2017 Water based homogenous carbon ink modified electrode as an efficient sensor system for simultaneous detection of ascorbic acid, dopamine and uric acid *Electrochim. Acta* **233** 92
54. Cai W, Lai T, Du H and Ye J 2014 Electrochemical determination of ascorbic acid, dopamine and uric acid based on exfoliated graphite paper electrode: A high performance flexible sensor *Sens. Actuat. B-Chem.* **193** 492
55. Yang L, Liu D, Huang J and You T 2014 Simultaneous determination of dopamine, ascorbic acid and uric acid at electrochemically reduced graphene oxide modified electrode *Sens. Actuat. B-Chem.* **193** 166